



**HAL**  
open science

## Geology of the Hokusai quadrangle (H05), Mercury

Jack Wright, David A Rothery, Matthew Balme, Susan J. Conway

► **To cite this version:**

Jack Wright, David A Rothery, Matthew Balme, Susan J. Conway. Geology of the Hokusai quadrangle (H05), Mercury. *Journal of Maps*, 2019, 15 (2), pp.509-520. 10.1080/17445647.2019.1625821 . hal-02268382

**HAL Id: hal-02268382**

**<https://hal.science/hal-02268382>**

Submitted on 20 Aug 2019

**HAL** is a multi-disciplinary open access archive for the deposit and dissemination of scientific research documents, whether they are published or not. The documents may come from teaching and research institutions in France or abroad, or from public or private research centers.

L'archive ouverte pluridisciplinaire **HAL**, est destinée au dépôt et à la diffusion de documents scientifiques de niveau recherche, publiés ou non, émanant des établissements d'enseignement et de recherche français ou étrangers, des laboratoires publics ou privés.



## Geology of the Hokusai quadrangle (H05), Mercury

Jack Wright, David A. Rothery, Matthew R. Balme & Susan J. Conway

To cite this article: Jack Wright, David A. Rothery, Matthew R. Balme & Susan J. Conway (2019) Geology of the Hokusai quadrangle (H05), Mercury, Journal of Maps, 15:2, 509-520, DOI: [10.1080/17445647.2019.1625821](https://doi.org/10.1080/17445647.2019.1625821)

To link to this article: <https://doi.org/10.1080/17445647.2019.1625821>



© 2019 The Author(s). Published by Informa UK Limited, trading as Taylor & Francis Group on behalf of Journal of Maps



[View supplementary material](#)



Published online: 17 Jun 2019.



[Submit your article to this journal](#)



[View Crossmark data](#)



## Geology of the Hokusai quadrangle (H05), Mercury

Jack Wright <sup>a</sup>, David A. Rothery <sup>a</sup>, Matthew R. Balme <sup>a</sup> and Susan J. Conway <sup>b</sup>

<sup>a</sup>School of Physical Sciences, The Open University, Milton Keynes, UK; <sup>b</sup>CNRS UMR 6112, Laboratoire de Planétologie et Géodynamique, Université de Nantes, Nantes, France

### ABSTRACT

The Hokusai (H05) quadrangle is in Mercury's northern mid-latitudes (0–90°E, 22.5–65°N) and covers almost 5 million km<sup>2</sup>, or 6.5%, of the planet's surface. We have used data from the MESSENGER spacecraft to make the first geological map of H05. Linework was digitized at 1:400,000-scale for final presentation at 1:3,000,000-scale, mainly using a ~166 m/pixel monochrome basemap. Three major photogeologic units of regional extent were mapped: intercrater, intermediate, and smooth plains. Materials of craters ≥ 20 km in diameter were classified according to their degradation state. Two classification schemes were employed in parallel, one with three classes and the other with five classes, for compatibility with existing MESSENGER-era quadrangle maps and the first global geologic map. This map will provide science context and targets for the ESA-JAXA BepiColombo mission to Mercury.

### ARTICLE HISTORY

Received 22 February 2019  
Revised 23 May 2019  
Accepted 24 May 2019

### KEYWORDS

Mercury; planetary geology; Hokusai; quadrangle; impact craters; planetary volcanism

## 1. Introduction

To date, Mercury has been the focus of two spacecraft missions: Mariner 10 (1974–1975; Dunne & Burgess, 1978) and MErcury, Surface, Space ENvironment, GEochemistry, and Ranging (MESSENGER; 2008–2015; Solomon, Nittler, & Anderson, 2018). Mercury has 15 latitudinally- and longitudinally-defined mapping quadrangles (Figure 1(b)). Following Mariner 10's flybys, 1:5,000,000 (1:5M) scale geological maps were made of the Borealis (H01; Grolier & Boyce, 1984), Victoria (H02; McGill & King, 1983), Shakespeare (H03; Guest & Greeley, 1983), Kuiper (H06; DeHon, Scott, & Underwood, 1981), Beethoven (H07; King & Scott, 1990), Tolstoj (H08; Schaber & McCauley, 1980), Discovery (H11; Trask & Dzursin, 1984), Michaelangelo (H12; Spudis & Prosser, 1984), and Bach (H15; Strom, Malin, & Leake, 1990) quadrangles. Hokusai (H05; 0–90°E, 22.5–65°N) was not mapped, as it was unimaged (Davies, Dornik, Gault, & Strom, 1978).

MESSENGER was the first spacecraft to image Mercury entirely (Solomon et al., 2018). This allowed the first global geological map of Mercury to be produced (1:15M-scale; Kinczyk et al., 2018). MESSENGER data resolution is sufficient for larger-scale (1:3M) quadrangle maps to be made. So far, H02 (Galluzzi et al., 2016), H03 (Guzzetta, Galluzzi, Ferranti, & Palumbo, 2017), and H04 (Mancinelli, Minelli, Pauselli, & Federico, 2016) have been published. Here, we present the first geological map of H05 (Main Map), which we began in October 2015.

## 2. Data

### 2.1. Basemaps

#### 2.1.1. Monochrome

The primary data for planetary photogeological mapping are monochrome image mosaic basemaps. MESSENGER's Mercury Dual Imaging System (MDIS; Hawkins et al., 2007) collected image data with its monochrome narrow-angle camera and multispectral wide-angle camera. With these, Chabot et al. (2016) created basemap mosaics with different illumination conditions covering the whole planet. The main basemaps we used to map H05 were its four version 0 ~166 m/pixel map-projected Basemap Reduced Data Record (BDR) tiles (Figure 1(a)), which are consistent with the basemaps of the other published MESSENGER-era quadrangle maps (Galluzzi et al., 2016; Guzzetta et al., 2017; Mancinelli et al., 2016). These tiles have moderate solar incidence angles (~68°; Chabot et al., 2016). Auxiliary basemaps for H05 with low incidence angles, for investigating surface reflectance variations (Figure 1(c)), and high incidence angles, with both western and eastern illumination, for enhancing subtle topographic features (Figure 1(d) and (e)), became available early during mapping (Chabot et al., 2016). Final, version 2, controlled basemaps for H05 were released after mapping was substantially underway (Denevi et al., 2018). Subsequent Mercury quadrangle maps are being constructed using these basemaps (Galluzzi et al., 2019).

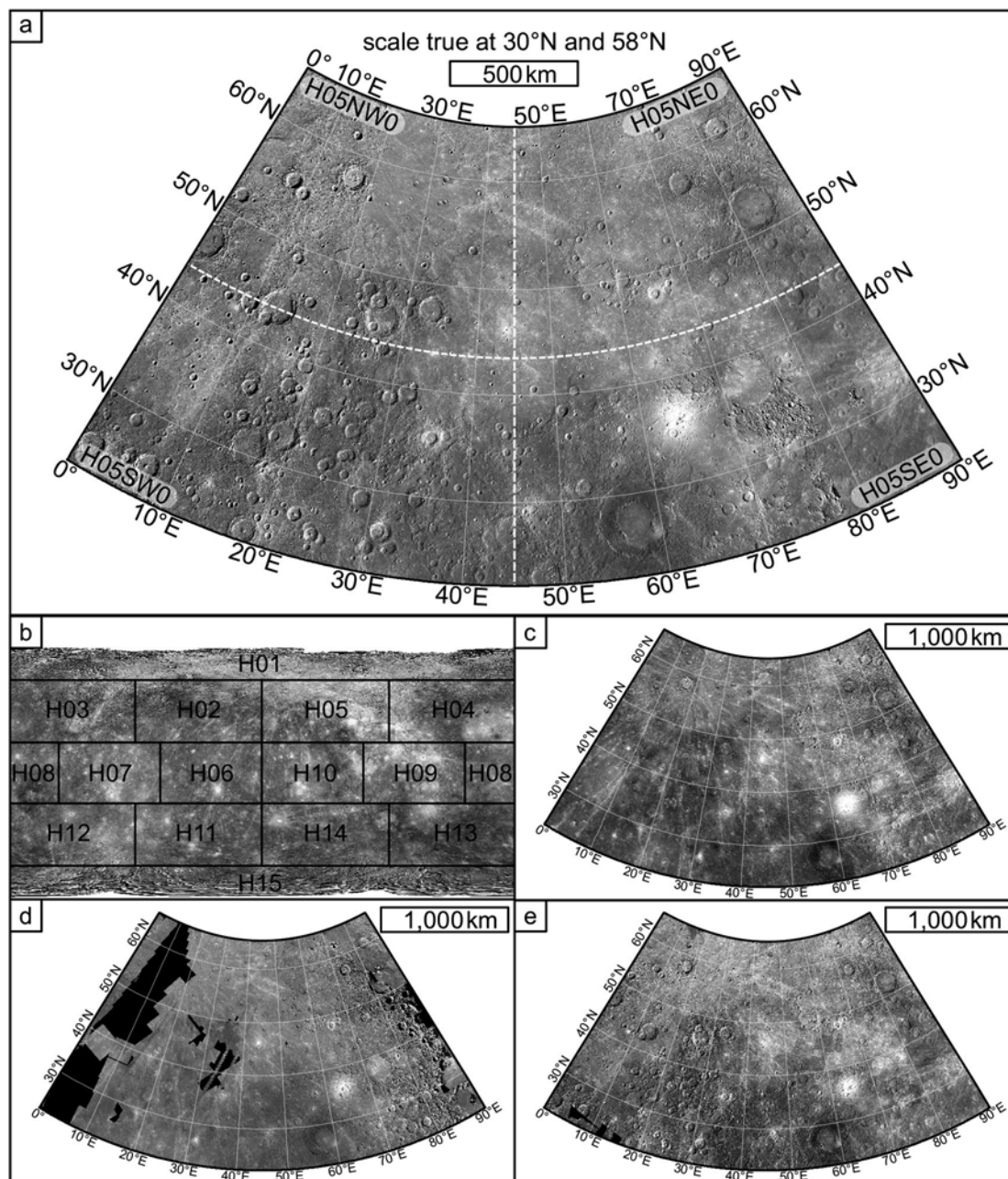


**Figure 1.** H05 basemaps. (a) Mosaic of the  $\sim 166$  m/pixel MDIS BDR basemap tiles. (b)  $\sim 665$  m/pixel global MDIS enhanced color mosaic (cylindrical projection; Denevi et al., 2016). Quadrangles are labeled and outlined. (c) Mosaic of the  $\sim 166$  m/pixel low-incidence angle basemap tiles. (d) Mosaic of the  $\sim 166$  m/pixel high-incidence angle (western) basemap tiles. (e) Mosaic of the high-incidence angle (eastern) basemap tiles. Panels (a) and (c–e) show H05’s native Lambert Conformal Conic projection (central meridian,  $45^\circ\text{E}$ ; standard parallels,  $30^\circ\text{N}$  and  $58^\circ\text{N}$ ). Monochrome products are by Chabot et al. (2016).

**2.1.1.1. Color.** Geomorphic units can sometimes be distinguished by color. We used the MESSENGER  $\sim 665$  m/pixel global enhanced color mosaic to inform our photogeological interpretations (Figure 1(b); Denevi et al., 2016). This was constructed using MDIS frames captured in the 430, 750, and 1000 nm bands. Principal component analyses were conducted by the MESSENGER team in this spectral space and they created the enhanced color mosaic by placing the second principal component, first principal component, and the 430/1000 ratio in the red, green, and blue channels, respectively (Denevi et al., 2009, 2016).

### 2.1.2. Topography

We used topographic data to aid mapping. Mercury Laser Altimeter (MLA; Cavanaugh et al., 2007) data created a digital elevation model (DEM) of Mercury’s northern hemisphere, encompassing H05 (Figure 2(a);  $\sim 665$  m/pixel; Zuber et al., 2012). MLA tracks diverge from the north, which means that this DEM suffers from interpolation uncertainties in southern H05. Shortly after mapping began, the first global stereo-DEM of Mercury was released (Figure 2(b);  $\sim 665$  m/pixel; Becker et al., 2016), which mitigated MLA DEM uncertainties. Later, an improved stereo-DEM of H05 was released with higher spatial resolution (Figure 2(c);

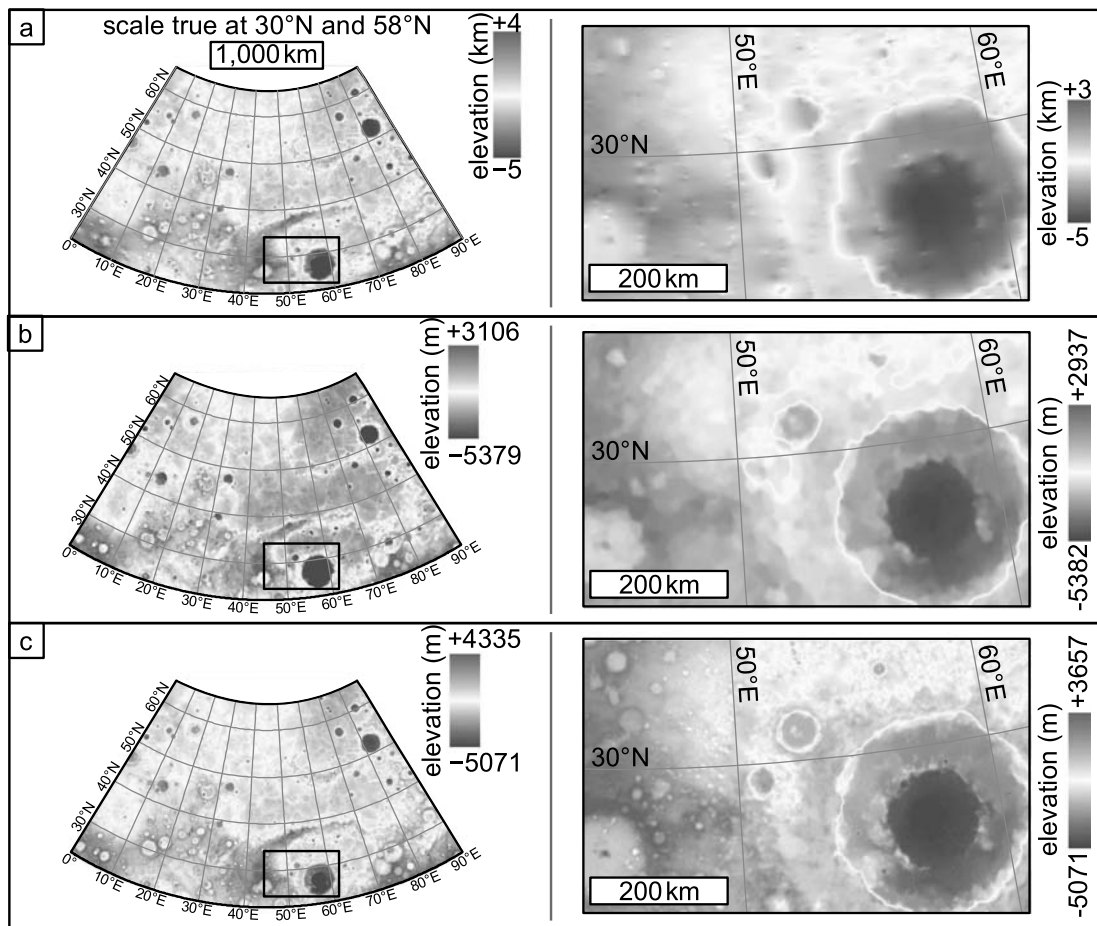


**Figure 2.** Topographic data for H05. Each panel (a–c) shows a quadrangle view (left) with a box indicating the location of the enlarged example (right). All panels show H05’s native Lambert Conformal Conic projection. (a)  $\sim 665$  m/pixel gridded MLA DEM (Zuber et al., 2012). (b)  $\sim 665$  m/pixel stereo-DEM (Becker et al., 2016). (c)  $\sim 222$  m/pixel stereo-DEM (Stark et al., 2017).

$\sim 222$  m/pixel; Stark et al., 2017). This became the primary source of topographic information for H05.

### 3. Methods

#### 3.1. Projection

H05, centered on  $45^{\circ}\text{E}$ , lies in Mercury’s northern mid-latitudes (Figure 1(b)). MESSENGER-era geological maps of the other quadrangles in this band were created in Lambert Conformal Conic (LCC) projections (standard parallels  $30^{\circ}\text{N}$  and  $58^{\circ}\text{N}$ ; Galluzzi et al., 2016; Guzzetta et al., 2017; Mancinelli et al., 2016). We mapped H05 in a LCC projection with identical standard parallels to facilitate future fusion of these maps (Figure 1(a); Galluzzi et al., 2019). The reference datum for this projected coordinate system is a sphere of radius 2,440 km; the published shape of Mercury when mapping began (Mazarico et al., 2014). We used the United States Geological Survey (USGS) Integrated Software for Imagers and Spectrometers version 3 (ISIS3) to reproject the raw basemaps.

#### 3.2. Scale

We prepared our map for publication at 1:3M-scale so it is compatible with the MESSENGER-era quadrangle

geological maps (Galluzzi et al., 2016; Guzzetta et al., 2017; Mancinelli et al., 2016). USGS guidance for planetary mappers recommends that digitization should be conducted at a scale  $\sim 4\times$  the publication scale (Skinner et al., 2018). Thus, a map to be published at 1:3M-scale should be digitized at  $\sim 1:750\text{k}$ -scale. An alternative recommendation is that the digitization scale should be  $2,000\times$  the basemap raster resolution (Tobler, 1987). Thus, the recommended digitization scale would be  $\sim 1:300\text{k}$ , because the basemap resolution is  $\sim 166$  m/pixel. Cognizant of these constraints, we digitized H05 at a scale of 1:400k.

#### 3.3. Digitization strategy

We digitized vector layers on the basemap raster layers in Esri ArcMap 10.1 Geographic Information System software. Primary digitizations belong to one of three feature classes: (1) geological contacts (polylines); (2) linear features (polylines), and; (3) surface features (polygons). Polylines and polygons are composed of geographically-located vertices linked by vector line segments. For mapping detail to be equal across H05, we digitized in vertex streaming mode, automatically creating vertices at equal intervals (‘stream tolerance’) as we moved the cursor over the basemap. We used a

stream tolerance of 300 m, which is approximately twice the basemap raster resolution, since no subpixel features can be resolved.

### 3.3.1. Contacts

Contacts on geological maps of Mercury mark the boundaries between geomorphic provinces and crater materials associated with individual impacts (Trask & Guest, 1975). We distinguished two ordinary contact types: (1) certain, where there is an easily located boundary between distinct geomorphic units, and; (2) approximate, where a contact between geomorphic units must exist, but its exact location is uncertain. Faults were included in the contacts feature class in anticipation of different geomorphic units occurring on opposite sides of a fault. We digitized the sharp breaks-in-slope at the bases of fault scarps. Our map contains two fault types: (1) thrust (certain), for well-defined fault breaks with obvious shortening kinematics, and; (2) thrust (uncertain), for features resembling thrusts but lacking unambiguous shortening kinematics. Provisions for other fault types were made, but all mapped faults ultimately conformed to one of the aforementioned fault types. This is consistent with the observation that widespread, large-scale extensional tectonics are not observed on Mercury (Byrne et al., 2014).

Geological units were generated from the contact feature class using ArcMap's 'Feature to Polygon' tool.

### 3.3.2. Linear features

All non-contact linear features were included within this feature class. Crater rims  $\geq 20$  km in diameter are symbolized with lines with double-hachures pointing into the crater. Crater rims  $\geq 5$  km and  $< 20$  km in diameter are symbolized with a simple line. Crater rim segments that have been subdued by impact ejecta, plains materials, or advanced degradation are shown with a dot-dash line. The brinks of irregular pits, interpreted as volcanic craters, are shown with lines with single-hachures pointing into the pit.

We mapped two classes of wrinkle ridges, small (lengths  $\leq 100$ s km, widths  $\sim 10$  km, heights  $\leq 1000$  m; Crane & Klimczak, 2019) tectonic landforms in Mercury's smooth plains caused by thrusting and folding: (1) common wrinkle ridges, which have no obvious alignments (Crane & Klimczak, 2019), and; (2) wrinkle ridge rings, which presumably overlie buried impact craters (Freed et al., 2012).

Other mapped linear features include small ridges and grabens within smooth plains hosted inside impact craters (Blair et al., 2013). Although these are almost certainly fault controlled, the faults cannot be resolved, or are too closely spaced to be rendered at the publication scale. Therefore we mapped the medial lines of these features.

### 3.3.3. Surface features

Surface features are textures through which the underlying, major photogeological unit(s) are visible. These include faculae (bright, relatively red, diffuse-edged materials interpreted as explosive volcanic deposits, often encompassing a pit; Goudge et al., 2014; Jozwiak, Head, & Wilson, 2018; Kerber et al., 2009, 2011; Murchie et al., 2008; Rothery, Thomas, & Kerber, 2014; Thomas, Rothery, Conway, & Anand, 2014a), hollows (steep-sided, flat-floored, irregular depressions,  $\sim 10$ s m deep, and  $\leq 100$ s km across, typically found within crater materials; Blewett et al., 2011, 2013; Thomas, Rothery, Conway, & Anand, 2014b), bright rays, and catenae (crater chains; Fegan, Rothery, Conway, & Anand, 2016). These are symbolized with ornaments to allow the host photogeological units, and their linework, to render, thus maximizing the information in the map.

## 4. Map description

### 4.1. Crater classifications

We grouped impact crater materials (ejecta, rims, terraces) according to their degradation state (e.g. Galluzzi et al., 2016; McGill & King, 1983). Under the assumptions that craters in the same degradation state formed approximately contemporaneously and degraded at similar rates, then degradation states convey the relative ages of non-overlapping craters. Following previous authors, the presence/absence of several photogeological features (bright rays, secondary crater fields, textured distal ejecta, crisp rims, wall terraces, internal peaks; Galluzzi et al., 2016; Kinczyk, Prockter, Chapman, & Susorney, 2016) were used to assign each crater  $\geq 20$  km in diameter a degradation class.

Mariner 10-era geological mappers classified craters into five degradation states ( $c_1$ – $c_5$ ; degraded–fresh; DeHon et al., 1981; Guest & Greeley, 1983; King & Scott, 1990; McGill & King, 1983; Schaber & McCauley, 1980; Spudis & Prosser, 1984; Strom et al., 1990; Trask & Dzursin, 1984). This stratigraphic numbering implies that  $c_1$  craters formed before  $c_2$  craters, etc. The MESSENGER-era global geological map of Mercury shows crater materials classified into five similar degradation states for craters  $\geq 40$  km in diameter (Kinczyk et al., 2018).

Previous MESSENGER-era quadrangle mappers used a three-class degradation system for craters  $\geq 20$  km in diameter (Galluzzi et al., 2016; Guzzetta et al., 2017; Mancinelli et al., 2016). These mappers wanted to construct a morphostratigraphy for their quadrangles where all craters in a fresher degradation state were also stratigraphically younger than any more-degraded crater. Some examples of degraded craters at the lower limit of classification were found

superposing fresher crater materials. In order to reconcile the apparent contradiction between crater morphology and stratigraphy, these mappers reduced the number of degradation classes from five to three. Classes  $C_3$  and  $C_1$  are for the freshest and most degraded craters, respectively, and craters of intermediate appearance are assigned the  $C_2$  class. Fewer classes made the classification more reproducible, allowing for successful merging of quadrangle maps (Galluzzi et al., 2019), and also eliminated examples of more-degraded craters overlying less-degraded craters.

Here, we used both classifications for craters  $\geq 20$  km in diameter, yielding two versions of our map to be compared with either the global geological map of Mercury (Kinczyk et al., 2018) or MESSENGER-era quadrangle geological maps (Galluzzi et al., 2016; Guzzetta et al., 2017; Mancinelli et al., 2016).

## 4.2. Mapped units

### 4.2.1. Intercrater plains (icp)

*Description:* The most widespread geomorphic unit on Mercury is the intercrater plains (Kinczyk et al., 2018; Trask & Guest, 1975; Whitten, Head, Denevi, & Solomon, 2014), described as ‘level to gently rolling ground between and around large craters and basins’ (Trask & Guest, 1975). Intercrater plains host both degraded and fresh craters. These plains have a high density of degraded secondary impact craters no longer attributable to a primary (Figure 3(a)). Secondary craters are bowl-shaped, or mature, with flat floors and subdued rims (Whitten et al., 2014). Intercrater plains have no striking color signature and generally coincide with the ‘intermediate terrain’ color unit (Figure 3(b); Denevi et al., 2009).

*Interpretation:* These plains are probably volcanic, but have been bombarded and mixed by impacts since their formation  $\sim 4$  Ga (Marchi et al., 2013; Whitten et al., 2014).

### 4.2.2. Intermediate plains (ip)

*Description:* Plains with a roughness intermediate between intercrater and smooth plains. Characterized by hummocky terrain composed of degraded crater rims with intervening low-lying regions with smooth, level surfaces (Figure 4(a)). Smooth patches constitute  $\sim 50\%$  of intermediate plains, which is a larger fraction of smooth material permissible within the definition of intercrater plains (Whitten et al., 2014). Qualitatively, these smooth patches have a similar superposing crater density to smooth plains. Often, the locations of the smooth patches are delimited by depressions caused by underlying impact craters. Intermediate plains generally have similar color properties to intercrater plains, but some smooth patches are brighter and redder, resembling smooth plains (Figure 4(b)). We mapped some larger smooth patches that occupy obvious crater

interiors, and are fully topographically confined, as smooth plains rather than grouping them within intermediate plains (Figure 4(c)). Nevertheless, many smooth patches are interconnected such that contacts separating them from hummocky regions would approach fractal complexity and would not render on the publication scale map. Thus, we mapped an intermediate plains unit defined by degraded-crater-controlled hummocky plains with intervening smooth patches.

*Interpretation:* Probably represent intercrater plains that have been partially inundated by smooth plains materials.

### 4.2.3. Smooth plains (sp)

*Description:* Smooth plains are widespread in H05 because it includes Borealis Planitia. In Borealis Planitia, smooth plains are characterized by a low density of superposing impact craters and abundant wrinkle ridges (Figure 5(a)). Superposing craters generally have textured ejecta blankets. Wrinkle ridges form linked networks that extend across much of Borealis Planitia. Borealis Planitia generally has sharp contacts with adjacent units. Borealis Planitia corresponds to the color terrain unit ‘high-reflectance red plains’ (Denevi et al., 2009), except in southwest H05 where it is ‘low-reflectance blue plains’ (Figure 5(b); Denevi et al., 2009). Elsewhere in H05, smooth plains exist in small patches within the other units, such as the floors of degraded secondary crater chains and volcanic vents. Here, contacts between smooth plains and surroundings are sometimes unclear. Sharply-defined smooth plains are also found in patches perched on the proximal ejecta of the craters Rachmaninoff and Rustaveli.

*Interpretation:* These extensive smooth plains probably formed  $\sim 3.8$ – $3.5$  Ga as the last voluminous volcanic effusions during Mercury’s history (Byrne et al., 2016; Denevi et al., 2013; Ostrach et al., 2015). Color variability could indicate compositional heterogeneity (Weider et al., 2015). Alternatively, small patches of smooth plains, particularly those perched on crater materials, are interpreted as ponded impact melt.

### 4.2.4. Crater materials

As we have used two crater degradation classifications, here we define the characteristics of the three-class system and then state further characteristics required for classification in the five-class system. We found no examples of more-degraded craters superposing less-degraded craters when implementing the five-class system.

*4.2.4.1. Fresh materials (three class— $C_3$ ; five class— $c_5$ ,  $c_4$ ).* Craters with sharp, complete crater rims, and well-defined terraces where present (Figure 6(a)). Internal uplift is crisp and intact. Wall, floor, and internal uplift



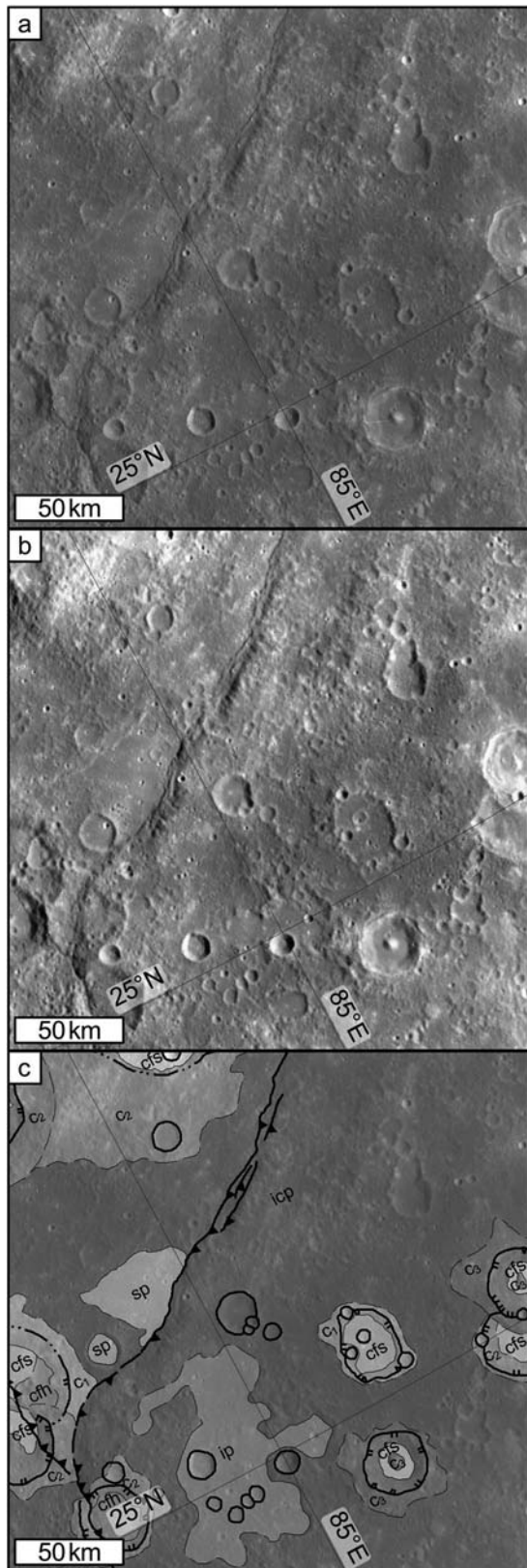


**Figure 3.** H05 intercrater plains. All panels show the same 1:3M-scale view in H05's native LCC projection. (a)  $\sim 166$  m/pixel BDR basemap. Intercrater plains, characterized by a high roughness and density of degraded craters, dominate this view. (b)  $\sim 665$  m/pixel enhanced color mosaic. Intercrater plains have variable color, but are generally darker than smooth plains. (c) Geologic map overlay on the  $\sim 166$  m/pixel BDR basemap. Intercrater plains (icp) have sharp contacts with smooth plains (sp) and uncertain contacts with intermediate plains (ip). See the Main Map for the key to the symbology in this figure.

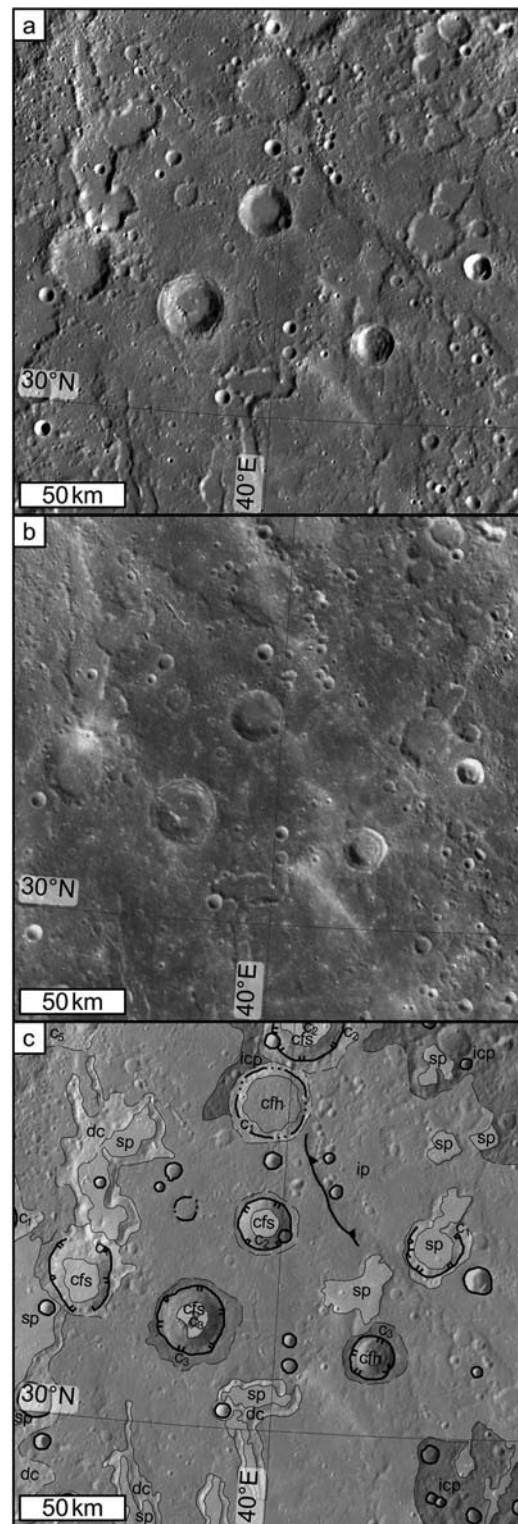


**Figure 4.** H05 intermediate plains. All panels show the same 1:3M-scale view in H05's native LCC projection. (a)  $\sim 166$  m/pixel BDR basemap. Intermediate plains are characterized by linked hummocky and smooth surfaces. (b)  $\sim 665$  m/pixel enhanced color mosaic. Intermediate plains have a color intermediate between intercrater and smooth plains. (c) Geologic map overlay on the  $\sim 166$  m/pixel BDR basemap. Intermediate plains (ip) contain topographically confined patches of smooth plains (sp). Contacts between smooth plains and intermediate plains are generally more certain, particularly when smooth plains is in contact with hummocky intermediate plains. Contacts between intercrater plains (icp) and intermediate plains are generally uncertain. See the Main Map for the key to the symbology in this figure.



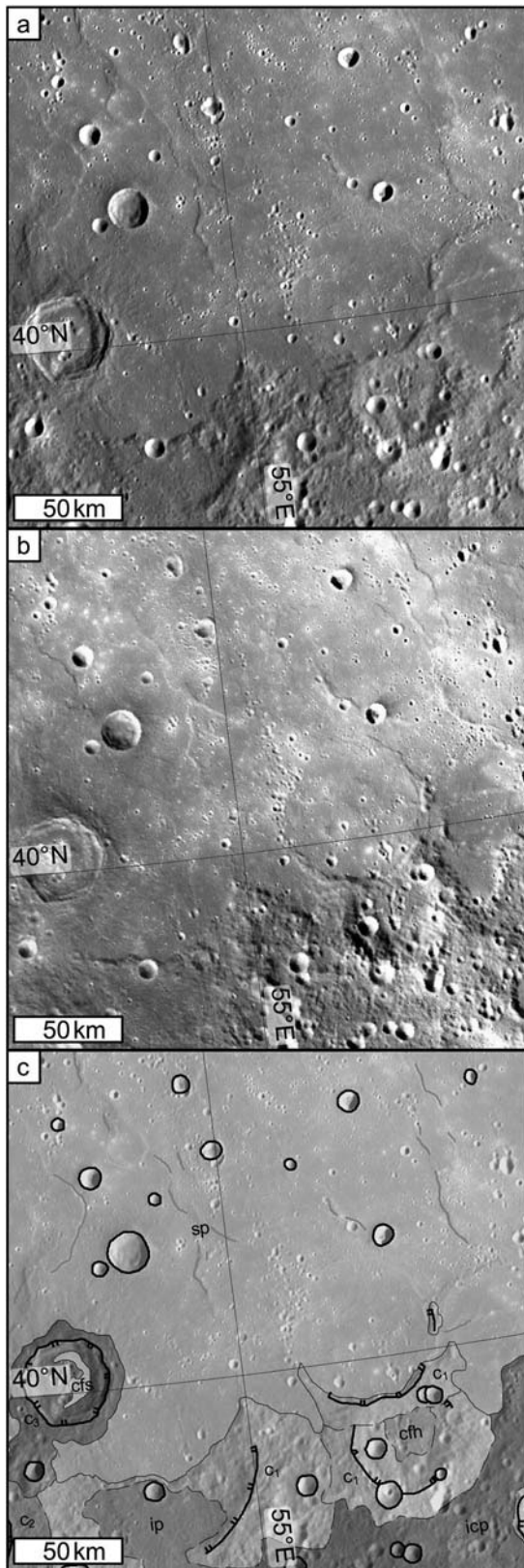


**Figure 5.** H05 smooth plains in Borealis Planitia. All panels show the same 1:3M-scale view in H05's native LCC projection. (a) ~166 m/pixel BDR basemap. Smooth plains are characterized smooth, level surfaces with a low density of craters. Superposing craters are relatively undegraded. (b) ~665 m/pixel enhanced color mosaic. Most smooth plains in Borealis Planitia are high-reflectance red plains (Denevi et al., 2009). Sharp color boundaries tend to match the geomorphic boundary between smooth plains and other plains. (c) Geologic map overlain on the ~166 m/pixel BDR basemap. Smooth plains (sp) have sharp contacts with intercrater plains (icp). See the Main Map for the key to the symbology in this figure.

contacts are distinct. Radially textured, relatively uncratered ejecta extends approximately one crater diameter from the rim. Radial catenae often present. Distal ejecta contacts are relatively distinct. Rays can be present. In the three-class system, such craters are classified as  $C_3$ . In the five-class system, they are  $c_5$  if rays are present (Figure 6(d) and (e)) or  $c_4$  otherwise (Figure 6(f) and (g)).

**4.2.4.2. Degraded materials (three class— $C_2$ ; five class— $c_3$ ).** Moderately degraded craters (Figure 6(b)). Rims are generally complete but not sharp. Terraces if present are not pristine. Central peaks/rings appear subdued. Ejecta is present but lacks radial texture. Distal ejecta contacts are uncertain. Such craters are classified as  $C_2$  in the three-class system, or  $c_3$  in the five-class system (Figure 6(h)).

**4.2.4.3. Heavily degraded materials (three class— $C_1$ ; five class— $c_2$ ,  $c_1$ ; dc).** Craters with incomplete rims, either from subsequent impacts or burial by plains materials (Figure 6(c)). Terraces are disrupted or absent. Wall-floor contacts are indistinct. Internal uplift is greatly subdued or absent. Distal ejecta is absent, except around impact basins > 100 km in diameter. In the three-class system, such craters are classified as  $C_1$ . In the five-class system, they are  $c_2$  (Figure 6(i)), they been breached by the surrounding plains, in which case they are  $c_1$  (Figure 6(j)). Degraded catenae (dc; Figure 6(k)) are a subset of the most degraded crater materials in each classification system. These are remnant rims of crater chains attributed to ancient basins (Fassett et al., 2012) that are the oldest features in evidence in H05.

**4.2.4.4. Smooth crater floor (cfs).** *Description:* Material geomorphically resembling smooth plains confined to crater floors.

*Interpretation:* In degraded craters it is probably post-impact volcanic plains. In fresh craters it could be solidified impact melt or post-impact volcanic plains.

**4.2.4.5. Hummocky crater floor (cfh).** *Description:* Rough textured or rolling material confined to crater floors.

*Interpretation:* In fresh craters this can often be ascribed to crater wall debris or impact-melt-free original floor materials. In more degraded craters, the rolling texture was caused by impact bombardment of the original crater floor.

### 4.3. Correlation of mapped units

Based on the stratigraphic relations recorded in the Main Maps, the crater classification correspondences in Section 4.2.4, and absolute model ages for plains

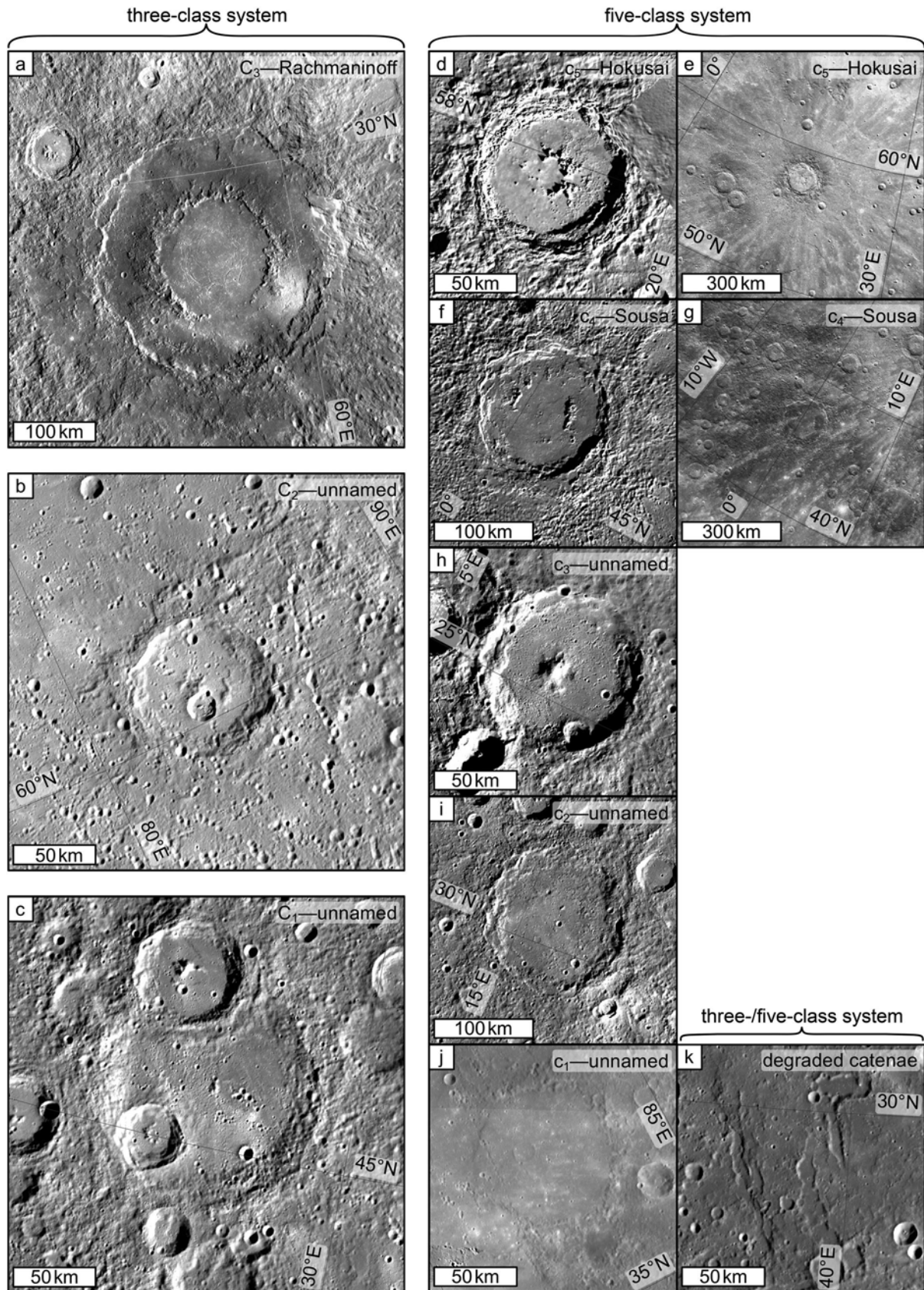


**Figure 6.** Craters typifying H05 crater degradation states. (a–c) The three-class system. (d–j) The five-class system. (k) Degraded catenae. All panels show H05's native LCC projection. All panels show the  $\sim 166$  m/pixel BDR basemap, except panels (e) and (g), which show the  $\sim 665$  m/pixel enhanced color mosaic to illustrate crater rays.

materials from other workers, we have constructed two schematic stratigraphies for H05: one based on the three-class crater degradation system and the other based on the five-class system (Figure 7).

The five-class system improves temporal resolution for crater formation, however it also improves the stratigraphic resolution of the map by bracketing the inter-crater plains. We found that  $c_3$  craters are unembayed

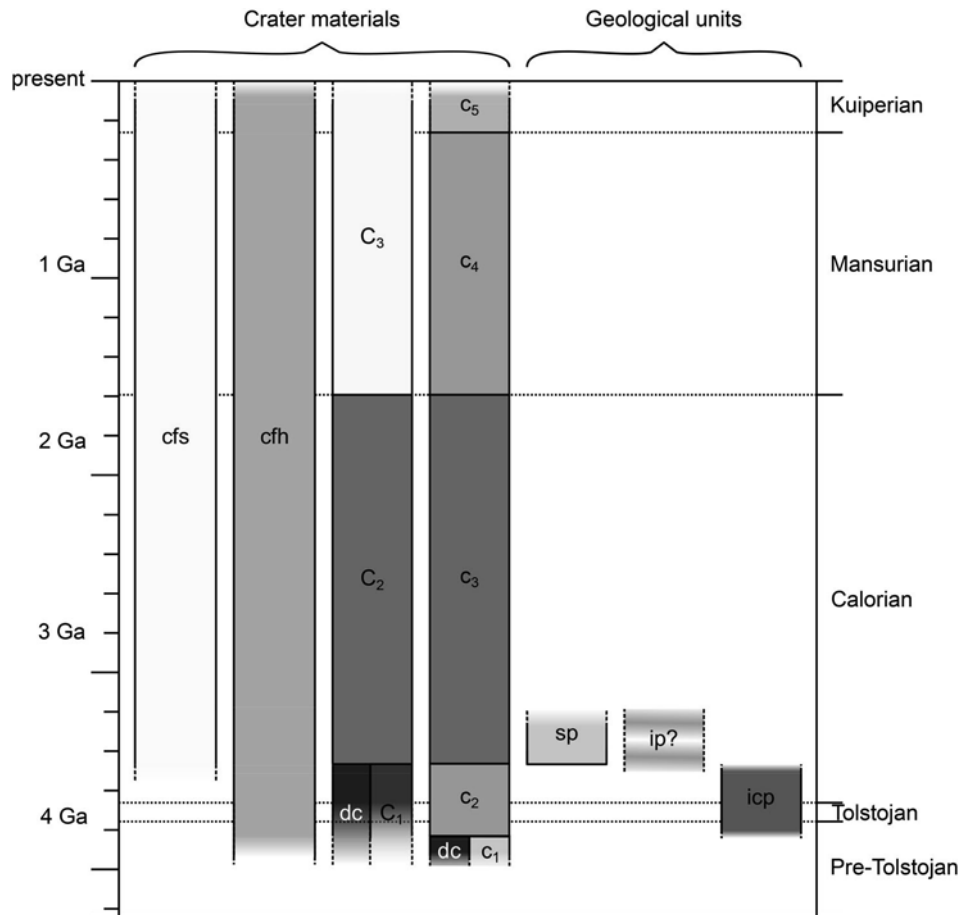


**Figure 7.** Schematic correlation of H05 map units from superposition relations, crater class correspondences, and absolute model age estimates of smooth plains (Byrne et al., 2016; Ostrach et al., 2015) and intercrater plains (Marchi et al., 2013; Whitten et al., 2014) across Mercury. The temporal extent of smooth plains represents large-volume plains only. Additional smooth plains include impact melt and late-stage volcanism that formed in disjointed geological instants over Mercury's history. The banded symbolization of intermediate plains represents uncertainty about their age relative to smooth plains. Mercury's time systems are at the right. Dotted lines indicate absolute model ages for these systems on the timescale at the left. Kuiperian and Mansurian basal ages are from Banks et al. (2017). Calorian and Tolstojan basal ages are from Spudis and Guest (1988). The base of the Pre-Tolstojan is undefined. See the Main Map for the key to the symbology used in this figure.

by intercrater plains, therefore  $c_3$  craters postdate the cessation of H05 intercrater plains formation. Similarly,  $c_1$  craters are embayed by intercrater plains where they are in contact, so  $c_1$  craters predate intercrater plains.

## 5. Conclusions

We used MESSENGER data to produce the first geological map of H05. One version is consistent with previous MESSENGER-era quadrangle geological maps of Mercury (Galluzzi et al., 2016; Guzzetta et al., 2017; Mancinelli et al., 2016). One important difference between these quadrangle maps, including our H05 map, and the first global geological map of Mercury, which is currently being prepared for submission (Kinczyk et al., 2018), is the inclusion of an intermediate plains unit that is texturally distinct from the intercrater plains and smooth plains common among all these maps. Our mapping suggests that the intermediate plains in H05 formed

during the same interval of geologic time as the quadrangle's smooth plains. A future, carefully conducted crater size-frequency distribution study could test this hypothesis.

We also produced an alternative version with five crater degradation classes corresponding to those on the global geological map. When employing the five-class system, we found no instances of more-degraded craters superposing less-degraded craters. This allows a morphostratigraphy of H05 with a higher temporal resolution than previous MESSENGER-era quadrangle maps. We recommend that future quadrangle mappers of Mercury implement the five-class system and the three-class system simultaneously, in case the five-class system can improve the stratigraphic resolution of their maps. Continued use of the three-class system will allow all the quadrangle maps to be merged in the future (Galluzzi et al., 2019).

This map completes 1:3M-scale mapping of Mercury's northern mid-latitudes, and it will be vital in providing science context and targets for the ESA-

JAXA BepiColombo mission to Mercury (Benkhoff et al., 2010; Rothery et al., 2010).

## Software

We used ESRI ArcMap 10.1 during map production. Basemaps were processed using USGS ISIS3. The Main Map was completed in Inkscape 0.91.

## Acknowledgements

We sincerely thank Valentina Galluzzi and David A. Williams for their insightful reviews of our manuscript. We are also grateful to Nick Scarle for his recommendations to clarify the visualization of the maps. The planetary data products used in this paper are publicly available from the Planetary Data System (PDS). MESSENGER data are credited to NASA/Johns Hopkins University Applied Physics Laboratory/Carnegie Institute of Washington.





## Disclosure statement

No potential conflict of interest was reported by the authors.

## Funding

This research was initially funded by the UK Science and Technology Facilities Council (STFC), and completed under Horizon 2020 grant 776276 'Planmap' (to whose mapping standards it conforms). Wright was funded by an Science and Technology Facilities Council PhD studentship (ST/N50421X/1) and is also grateful to the British Society for Geomorphology, UK Remote Sensing and Photogrammetry Society, and Royal Astronomical Society for providing additional funding during the completion of this study.

## ORCID

Jack Wright  <http://orcid.org/0000-0003-0481-0863>  
David A. Rothery  <http://orcid.org/0000-0002-9077-3167>  
Matthew R. Balme  <http://orcid.org/0000-0001-5871-7475>  
Susan J. Conway  <http://orcid.org/0000-0002-0577-2312>

## References

- Banks, M. E., Xiao, Z., Braden, S. E., Barlow, N. G., Chapman, C. R., Fassett, C. I., & Marchi, S. S. (2017). Revised constraints on absolute age limits for Mercury's Kuiperian and Mansurian stratigraphic systems. *Journal of Geophysical Research: Planets*, *122*, 1010–1020.
- Becker, K. J., Robinson, M. S., Becker, T. L., Weller, L. A., Edmundson, K. L., Neumann, G. A., ... Solomon, S. C. (2016). First global digital elevation model of Mercury. *47th Lunar and Planetary Science Conference*, The Woodlands, Houston, p. Abstract #2959.
- Benkhoff, J., van Casteren, J., Hayakawa, H., Fujimoto, M., Laakso, H., Novara, M., ... Ziethe, R. (2010). Bepicolombo—comprehensive exploration of Mercury: Mission overview and science goals. *Planetary and Space Science*, *58*, 2–20.
- Blair, D. M., Freed, A. M., Byrne, P. K., Klimczak, C., Prockter, L. M., Ernst, C. M., ... Zuber, M. T. (2013). The origin of graben and ridges in Rachmaninoff, Raditladi, and Mozart basins, Mercury. *Journal of Geophysical Research: Planets*, *118*, 47–58.
- Blewett, D. T., Chabot, N. L., Denevi, B. W., Ernst, C. M., Head, J. W., Izenberg, N. R., ... Hurwitz, D. M. (2011). Hollows on Mercury: MESSENGER evidence for geologically recent volatile-related activity. *Science*, *333*, 1856–1859.
- Blewett, D. T., Vaughan, W. M., Xiao, Z., Chabot, N. L., Denevi, B. W., Ernst, C. M., ... Solomon, S. C. (2013). Mercury's hollows: Constraints on formation and composition from analysis of geological setting and spectral reflectance. *Journal of Geophysical Research: Planets*, *118*, 1013–1032.
- Byrne, P. K., Klimczak, C., Şengör, A. M. C., Solomon, S. C., Watters, T. R., & Hauck, S. A. (2014). Mercury's global contraction much greater than earlier estimates. *Nature Geoscience*, *7*, 301–307.
- Byrne, P. K., Ostrach, L. R., Fassett, C. I., Chapman, C. R., Denevi, B. W., Evans, A. J., ... Solomon, S. C. (2016). Widespread effusive volcanism on Mercury likely ended by about 3.5 Ga. *Geophysical Research Letters*, *43*, 7408–7416.
- Cavanaugh, J. F., Smith, J. C., Sun, X., Bartels, A. E., Ramos-Izquierdo, L., Krebs, D. J., ... Smith, D. E. (2007). The Mercury Laser Altimeter instrument for the MESSENGER mission. *Space Science Reviews*, *131*, 451–479.
- Chabot, N. L., Denevi, B. W., Murchie, S. L., Hash, C. D., Ernst, C. M., Blewett, D. T., ... Solomon, S. C. (2016). Mapping Mercury: Global imaging strategy and products from the MESSENGER mission. *47th Lunar and Planetary Science Conference*, The Woodlands, Houston, p. 1256.
- Crane, K. T., & Klimczak, C. (2019). Tectonic patterns of shortening landforms in Mercury's northern smooth plains. *Icarus*, *317*, 66–80.
- Davies, M. E., Dornik, S. E., Gault, D. E., & Strom, R. G. (1978). Atlas of Mercury, NASA Special Publication.
- DeHon, R. A., Scott, D. H., & Underwood, J. R. (1981). Geologic map of the Kuiper quadrangle of Mercury. USGS Misc. Investig. Ser. Map I-1233.
- Denevi, B. W., Chabot, N. L., Murchie, S. L., Becker, K. J., Blewett, D. T., Domingue, D. L., ... Solomon, S. C. (2018). Calibration, projection, and final image products of MESSENGER's Mercury Dual Imaging system. *Space Science Reviews*, *214*, 1–52.
- Denevi, B. W., Ernst, C. M., Meyer, H. M., Robinson, M. S., Murchie, S. L., Whitten, J. L., ... Peplowski, P. N. (2013). The distribution and origin of smooth plains on Mercury. *Journal of Geophysical Research: Planets*, *118*, 891–907.
- Denevi, B. W., Robinson, M. S., Solomon, S. C., Murchie, S. L., Blewett, D. T., Domingue, D. L., ... Chabot, N. L. (2009). The evolution of Mercury's crust: A global perspective from MESSENGER. *Science*, *324*, 613–618.
- Denevi, B. W., Seelos, F. P., Ernst, C. M., Keller, M. R., Chabot, N. L., Murchie, S. L., ... Blewett, D. T. (2016). Final calibration and multispectral map products from the Mercury Dual Imaging System Wide-Angle Camera on MESSENGER. *47th Lunar and Planetary Science Conference*, The Woodlands, Houston, p. 1264.
- Dunne, J. A., & Burgess, E. (1978). The voyage of Mariner 10, NASA Special Publication.
- Fassett, C. I., Head, J. W., Baker, D. M. H., Zuber, M. T., Smith, D. E., Neumann, G. A., ... Preusker, F. (2012). Large impact basins on Mercury: Global distribution, characteristics, and modification history from

- MESSENGER orbital data. *Journal of Geophysical Research: Planets*, 117, E00L08. doi:10.1029/2012JE004154
- Fegan, E. R., Rothery, D. A., Conway, S. J., & Anand, M. (2016). Mercury catenae: Linear features and lighting bias. *47th Lunar and Planetary Science Conference*, The Woodlands, Houston, p. Abstract #2945.
- Freed, A. M., Blair, D. M., Watters, T. R., Klimczak, C., Byrne, P. K., Solomon, S. C., ... Melosh, H. J. (2012). On the origin of graben and ridges within and near volcanically buried craters and basins in Mercury's northern plains. *Journal of Geophysical Research: Planets*, 117, 1–15.
- Galluzzi, V., Giacomini, L., Guzzetta, L., Lewang, A. M., Malliband, C. C., Mancinelli, P., ... Rothery, D. A. (2019). Geological mapping of Mercury. *Geophysical research abstracts*.
- Galluzzi, V., Guzzetta, L., Ferranti, F., Di Achille, G., Rothery, D. A., & Palumbo, P. (2016). Geology of the Victoria quadrangle (H02), Mercury. *Journal of Maps*, 12, 227–238.
- Goudge, T. A., Head, J. W., Kerber, L., Blewett, D. T., Denevi, B. W., Domingue, D. L., ... Solomon, S. C. (2014). Global inventory and characterisation of pyroclastic deposits on Mercury: New insights into pyroclastic activity from MESSENGER orbital data. *Journal of Geophysical Research: Planets*, 119, 635–658.
- Grolier, M. J., & Boyce, J. M. (1984). Geologic map of the Borealis region (H-1) of Mercury. USGS Misc. Investig. Ser. Map I-1660.
- Guest, J. E., & Greeley, R. (1983). Geologic map of the Shakespeare (H-3) quadrangle of Mercury. USGS Misc. Investig. Ser. Map I-1408.
- Guzzetta, L., Galluzzi, V., Ferranti, L., & Palumbo, P. (2017). Geology of the Shakespeare quadrangle (H03), Mercury. *Journal of Maps*, 13, 227–238.
- Hawkins, S. E., Boldt, J. D., Darlington, E. H., Espiritu, R., Gold, R. E., Gotwols, B., ... Williams, B. D. (2007). The Mercury Dual Imaging system on the MESSENGER spacecraft. *Space Science Reviews*, 131, 247–338.
- Jozwiak, L. M., Head, J. W., & Wilson, L. (2018). Explosive volcanism on Mercury: Analysis of vent and deposit morphology and modes of eruption. *Icarus*, 302, 191–212.
- Kerber, L., Head, J. W., Blewett, D. T., Solomon, S. C., Wilson, L., Murchie, S. L., ... Domingue, D. L. (2011). The global distribution of pyroclastic deposits on Mercury: The view from MESSENGER flybys 1-3. *Planetary and Space Science*, 59, 1895–1909.
- Kerber, L., Head, J. W., Solomon, S. C., Murchie, S. L., Blewett, D. T., & Wilson, L. (2009). Explosive volcanic eruptions on Mercury: Eruption conditions, magma volatile content, and implications for interior volatile abundances. *Earth and Planetary Science Letters*, 285, 263–271.
- Kinczyk, M. J., Prockter, L. M., Byrne, P. K., Denevi, B. W., Ostrach, L. R., & Skinner, J. A. (2018). A global geological map of Mercury. *Mercury: Current and future science of the innermost planet*, Columbia, Maryland, p. Abstract #6123.
- Kinczyk, M. J., Prockter, L. M., Chapman, C. R., & Susorney, H. C. M. (2016). A morphological evaluation of crater degradation on Mercury: Revisiting crater classification with MESSENGER data. *47th Lunar and Planetary Science Conference*, The Woodlands, Houston, p. Abstract #1573.
- King, J. S., & Scott, D. H. (1990). Geologic map of the Beethoven quadrangle of Mercury. USGS Misc. Investig. Ser. Map I-2048.
- Mancinelli, P., Minelli, F., Pauselli, C., & Federico, C. (2016). Geology of the Raditladi quadrangle, Mercury (H04). *Journal of Maps*, 5647, 1–13.
- Marchi, S., Chapman, C. R., Fassett, C. I., Head, J. W., Bottke, W. F., & Strom, R. G. (2013). Global resurfacing of Mercury 4.0–4.1 billion years ago by heavy bombardment and volcanism. *Nature*, 499, 59–61.
- Mazarico, E., Genova, A., Goossens, S., Lemoine, F. G., Neumann, G. A., Zuber, M. T., ... Solomon, S. C. (2014). The gravity field, orientation, and ephemeris of Mercury from MESSENGER observations after three years in orbit. *Journal of Geophysical Research: Planets*, 119, 2417–2436.
- McGill, G. E., & King, E. A. (1983). Geologic map of the Victoria (H-2) quadrangle of Mercury. USGS Misc. Investig. Ser. Map I-1409.
- Murchie, S. L., Watters, T. R., Robinson, M. S., Head, J. W., Strom, R. G., Chapman, C. R., ... Blewett, D. T. (2008). Geology of the Caloris basin, Mercury: A view from MESSENGER. *Science*, 321, 73–76.
- Ostrach, L. R., Robinson, M. S., Whitten, J. L., Fassett, C. I., Strom, R. G., Head, J. W., & Solomon, S. C. (2015). Extent, age, and resurfacing history of the northern smooth plains on Mercury from MESSENGER observations. *Icarus*, 250, 602–622.
- Rothery, D. A., Marinangeli, L., Anand, M., Carpenter, J., Christensen, U., Crawford, I. A., ... Wurz, P. (2010). Mercury's surface and composition to be studied by BepiColombo. *Planetary and Space Science*, 58, 21–39.
- Rothery, D. A., Thomas, R. J., & Kerber, L. (2014). Prolonged eruptive history of a compound volcano on Mercury: Volcanic and tectonic implications. *Earth and Planetary Science Letters*, 385, 59–67.
- Schaber, G. G., & McCauley, J. F. (1980). Geologic map of the Tolstoj quadrangle of Mercury (H-8). Map I-1199. USGS Misc. Investig. Ser. Map I-1199.
- Skinner, J. A., Huff, A. E., Fortezzo, C. M., Gaither, T. A., Hare, T. M., & Hunter, M. A. (2018). Planetary geologic mapping protocol.
- Solomon, S. C., Nittler, L. R., & Anderson, B. J. (2018). *Mercury: The view after MESSENGER*. Cambridge: Cambridge University Press.
- Spudis, P. D., & Guest, J. E. (1988). Stratigraphy and geologic history of Mercury. In F. Vilas, C. R. Chapman, & M. S. Matthews (Eds.), *Mercury* (pp. 118–164). Tucson: University of Arizona Press.
- Spudis, P. D., & Prosser, J. G. (1984). Geologic map of the Michelangelo quadrangle of Mercury. USGS Misc. Investig. Ser. Map I-1659.
- Stark, A., Preusker, F., Oberst, J., Matz, K.-D., Gwinner, K., & Roatsch, T. (2017). High-resolution topography from MESSENGER orbital stereo imaging - the H5 quadrangle "Hokusai". *48th Lunar and Planetary Science Conference*, The Woodlands, Houston, p. Abstract #2287.
- Strom, R. G., Malin, M. C., & Leake, M. A. (1990). Geologic map of the Bach region of Mercury. USGS Misc. Investig. Ser. Map I-2015.
- Thomas, R. J., Rothery, D. A., Conway, S. J., & Anand, M. (2014a). Mechanisms of explosive volcanism on Mercury: Implications from its global distribution and morphology. *Journal of Geophysical Research: Planets*, 119, 2239–2254.
- Thomas, R. J., Rothery, D. A., Conway, S. J., & Anand, M. (2014b). Hollows on Mercury: Materials and mechanisms involved in their formation. *Icarus*, 229, 221–235.

- Tobler, W. (1987). Measuring spatial resolution. *Proceedings of the land resource information systems conference*, Beijing, pp. 12–16.
- Trask, N. J., & Dzurisin, D. (1984). Geologic map of the Discovery (H-11) quadrangle of Mercury. USGS Misc. Investig. Ser. Map I-1658.
- Trask, N. J., & Guest, J. E. (1975). Preliminary geologic terrain map of Mercury. *Journal of Geophysical Research*, 80, 2461–2477.
- Weider, S. Z., Nittler, L. R., Starr, R. D., Crapster-Pregont, E. J., Peplowski, P. N., Denevi, B. W., ... Solomon, S. C. (2015). Evidence for geochemical terranes on Mercury: Global mapping of major elements with MESSENGER's X-Ray Spectrometer. *Earth and Planetary Science Letters*, 416, 109–120.
- Whitten, J. L., Head, J. W., Denevi, B. W., & Solomon, S. C. (2014). Intercrater plains on Mercury: Insights into unit definition, characterization, and origin from MESSENGER datasets. *Icarus*, 241, 97–113.
- Zuber, M. T., Smith, D. E., Phillips, R. J., Solomon, S. C., Neumann, G. A., Hauck, S. A., ... Yang, D. (2012). Topography of the northern hemisphere of Mercury from MESSENGER laser altimetry. *Science*, 336, 217–220.